Supporting Information: Controlling cargo trafficking in multicomponent membranes

Tine Curk[1,2], Peter Wirnsberger[3], Jure Dobnikar[1,3], Daan Frenkel[3], Anđela Šarić[4,*]

[1]*Institute of Physics, Chinese Academy of Sciences,*
Beijing, China
[2]*Department of Chemistry, University of Maribor,*
Maribor, Slovenia
[3]*Department of Chemistry,*
University of Cambridge,
Cambridge, UK
[4]*Department of Physics and Astronomy,*
Institute for the Physics of Living Systems
University College London, London, UK
*

This Supporting Information provides details of the theoretical derivation of the mean field model (Section I), the simulation procedures (Section II), the procedure for determining the Gaussian stiffness (Section III), and supporting results and figures (Section IV).

I. ANALYTICAL MODEL DERIVATION

We consider a fluid membrane discretised into small patches of size $a^2 \approx 25 nm^2$. Each patch represents one component. Different component types are denoted by an index $_j$ and the membrane is defined by a unit composition vector $\mathbf{f} = [f_1, f_2, f_3, ...]$ specifying the fractions of different component types within the membrane. Components can represent membrane lipids, embedded transmembrane receptors, or inert membrane proteins. Each component type also has a spontaneous curvature $c_{0,j}$ and (mean and Gaussian) bending rigidity moduli κ_j, $\bar{\kappa}_j$ associated with it.

A. Curvature free energy

The theory is based on a Helfrich Hamiltonian for the curvature free energy density:

$$H_c = \frac{\kappa}{2}(2C - c_0)^2 + \bar{\kappa} K \ , \tag{1}$$

with C and K the local mean and Gaussian curvature of the membrane, and c_0 the local preferred curvature. The total elastic free energy of a membrane of size A is usually obtained by integrating Eq. (1),

$$F_c = \int H_c \, dA \ . \tag{2}$$

Such integral form implies a strong assumption of locality: all variables pertinent to the elastic free energy are local. The integral form is valid as a macroscopic (thermodynamic) descriptor of an elastic membrane. On a microscopic level however, the atomistic nature implies that the above integral should be computed as a sum over individual discreet building blocks.

The lipid bilayer membrane is made of finite sized components – lipids. The thickness of the bilayer is around 5nm, therefore, the smallest length scale, where the local picture of the Helfrich integral is expected to apply, is of the order of membrane thickness $a = 5$nm. We discretise the Hefrich integral into a sum over N components of size a^2

$$F_c = \sum_{j'}^{N} H_{c,j'} \, a^2 \ , \tag{3}$$

---

*Electronic address: `a.saric@ucl.ac.uk;Telephone:+442076797295`

with $H_{c,j'}$ the curvature free energy density of component j', Eq. (1). An implicit assumption remains: neighbouring components in the membrane are independent. We have not specified the nature of the component, it could represent a lipid patch, a protein surrounded with a few lipids or a protein cluster, for example. The component size could also be larger than 5nm, however, in that case the component does not directly map to a transmembrane protein, but a multitude of proteins and lipids. Choosing the component size at the lower limit (5nm) ensures that each component contains at most a few closely packed proteins; lateral extension of a transmembrane proteins typically being around 2nm. For simplicity we use a picture where each component represents either pure lipids or a single transmembrane protein (surrounded by a few lipids), but the theory can be applied also to multi-protein components.

B. Mean field

In the system under study the membrane is either flat or wrapped around a particle. In the following we assume a constant mean curvature approximation: the mean curvature of each component of the membrane is a constant and fully determined by the shell radius: $C_j = -1/R_{\mathrm{w}}$. Equivalently for the flat membrane the mean curvature of all components is zero: $C = 0$. This approximation amounts to neglecting correlations between local mean curvature and spontaneous curvature of the membrane. For example a stoichiometric mixture of components with equal positive and negative spontaneous curvatures in a flat membrane would yield an overall flat membrane of zero mean curvature. However, the mean-field formalism constrains every component of a flat membrane to a zero mean curvature and the free energy is overstated. In the following, all bending moduli are assumed to be the same: $\kappa = \kappa_j$ and $\bar{\kappa} = \bar{\kappa}_j$. If the bending moduli are not the same the mean curvature C_j would not only be correlated to the spontaneous curvature $c_{0,j}$, but also to the bending rigidity κ_j, which would lead to further deviation of the optimal membrane shape from the perfectly spherical shell assumed in the mean-field picture.

The membrane contains a mixture of multiple types of components. Because all components are assumed to have the same imposed mean and Gaussian curvature, $C_{j'} = C$ and $K_{j'} = K$, Eq. (3) can be equally written as a sum over n component types j

$$F_c = \sum_j^n N_j H_{c,j} \, a^2 = N \sum_j^n f_j H_{c,j} \, a^2 \, , \tag{4}$$

with N_j the number of components of type j present in the membrane, $N = \sum_j N_j$ the total number of components and the component composition fractions $f_j = N_j/N$. We use the notation where prime indices j' refer to a specific component located in the membrane, while normal indices j denote a component type. The elastic mean-field free energy of a membrane size A with curvature C, using Eqs. (1) and (4), is

$$F_c(A, C, K) = A \sum_j^n f_j \left[\frac{\kappa}{2} (2C - c_{0,j})^2 + \bar{\kappa} K \right] \, . \tag{5}$$

C. Mean field 2: alternative approach.

An alternative approach would relax the requirement that the membrane mean curvature is imposed on every component. Instead, the mean curvature is imposed only "on average" over all components in the membrane. This limit assumes no penalty to spatial mean curvature fluctuations: Eqs. (1) and (2) are applied directly to a total membrane patch area A. This is equivalent to Eq. (4) with a single large "component" of size A. The spontaneous curvature of the total patch is defined as the average over individual component spontaneous curvatures

$$\langle c_0 \rangle = \frac{1}{N} \sum_{j'}^N c_{0,j'} = \sum_j^n f_j c_{0,j} \, , \tag{6}$$

with f_j the membrane composition vector. Similarly for the mean square spontaneous curvature: $\langle c_0^2 \rangle = \sum_j^n f_j c_{0,j}^2$. The Hellfrich expression (3) using the mean spontaneous curvature becomes

$$\tilde{F}_c(A, C, K)/A = \frac{\kappa}{2} (2C - \langle c_0 \rangle)^2 + \bar{\kappa} K = \frac{\kappa}{2} \left(4C^2 - 4C\langle c_0 \rangle + \langle c_0 \rangle^2 \right) + \bar{\kappa} K \, . \tag{7}$$

We compare the above result to the previous mean-field expression (Eq. (5)) applied to a membrane area A:

$$F_c(A, C, K)/A = \sum_j^n f_j \left[\frac{\kappa}{2}(4C^2 - 4Cc_{0,j} + c_{0,j}^2) + \bar{\kappa}K \right] = \frac{\kappa}{2} \left(4C^2 - 4C\langle c_0 \rangle + \langle c_0^2 \rangle \right) + \bar{\kappa}K \ , \qquad (8)$$

These two free energy expressions are related through a fluctuation term

$$\tilde{F}_c(A, C, K) = F_c(A, C, K) - A\frac{\kappa}{2} \left(\langle c_0 \rangle^2 - \langle c_0^2 \rangle \right) \ . \qquad (9)$$

Importantly, the above fluctuation term refers to spatial fluctuations in the spontaneous curvature of membrane components. It does not refer to mean curvature of the membrane; thermal fluctuations of the local membrane bending are implicitly included in the starting Helfrich expression, Eq. (1).

The two mean-field expression, Eqs. (7) and (8), conveniently provide a lower and upper bound to the free energy of the membrane patch of size A with some average imposed mean and Gaussian curvature C and K. The upper bound (8) is reached in the limit of an infinite membrane surface tension (curvature imposed on every component), while the lower bound (8) is realised in the case of an 1D membrane (a chain of components) with zero surface tension (total curvature of the membrane imposed only at the boundary). For a 2D membrane with zero surface tension the geometric constraints on bending likely prevent the lower bound of being reached. Entropy of partial ordering of components affects the 2D membrane, but not the 1D chain, because any permutation of components along a chain will result in the same curvature energy (unless the curvature is so large that the chain folds onto itself).

In the following the upper estimate for the mean-field free energy (Eq. (5)) will be used for all theoretical predictions. The reason for this choice is that the nanoparticle binds to the membrane via receptor attachments and the membrane envelope will likely be tightly wrapped around the particle.

D.   Endocytosis free energy

We attempt to analytically calculate the free energy change upon a particle endocytosis. As stated above, the membrane is composed of different component types with a component vector $\mathbf{f}$ and spontaneous curvature vector $\mathbf{c}_0$ specifying the spontaneous curvature of all component types. Additionally each component type also has an interaction with a particle captured by the vector $\boldsymbol{\epsilon}$. We assume a simple square well interaction potential where $\boldsymbol{\epsilon}$ specifies the well depth. The surface tension and density ρ of the membrane is assumed to be constant. All three vectors $(\mathbf{f}, \mathbf{c}_0, \boldsymbol{\epsilon})$ are of length n with n the number of distinct components in the membrane.

The following notation is used:

- e.g. $A, N, \mathbf{f}$ – standard letters refer to the initial flat membrane *before* endocytosis

- e.g. $\tilde{A}, \tilde{N}, \tilde{\mathbf{f}}$ – letters with a tilde refer to the membrane that remains flat *after* the full endocytosis has taken place

- e.g. $A_w, N_w, \mathbf{f}^w$ – letters with $_w$ script refer to the membrane wrapped around the particle *after* the full endocytosis has taken place.

Initially, the membrane is flat with a total area A and $\mathbf{f}$ is the component composition in the membrane. Upon particle endocytosis a small membrane area $A_w = 4\pi R_w^2$ is wrapped around a particle with a membrane shell radius R_w. The remaining membrane area $\tilde{A} = A - A_w$ remains flat. The composition of the wrapped part $\mathbf{f}^w$ is in general different from the remaining flat membrane $\tilde{\mathbf{f}}$. Therefore, the two conservation laws are: Area conservation

$$A = \tilde{A} + A_w \qquad (10)$$

and component number conservation: $N = \tilde{N} + N_w$, which applies to every component type, hence,

$$\mathbf{f}A = \tilde{\mathbf{f}}\tilde{A} + \mathbf{f}^w A_w \ . \qquad (11)$$

We have assumed that the membrane surface tension and 2D component density $\rho = \frac{N}{A} = \frac{\tilde{N}}{\tilde{A}} = \frac{N_w}{A_w} = const.$ remains unchanged during the endocytosis.

Furthermore, we assume that lateral component diffusion is fast compared to the endocytosis timescale. Under these conditions the components can be treated as independently adsorbing to the particle. The process of endocytosis is rather complicated, however, we are only interested in the free energy change between the initial and final state. We assume that during all of the endocytosis process the (partially) wrapped part of the membrane is in contact with the remainder of the membrane (the reservoir). Therefore, the wrapped components composition is given by the generalised Langmuir adsorption isotherm:

$$f_j^{\mathrm{w}} = \frac{e^{\beta(\tilde{\mu}_j - F_{c,j}(R_{\mathrm{w}}) - \epsilon_j)}}{\sum_j e^{\beta(\tilde{\mu}_j - F_{c,j}(R_{\mathrm{w}}) - \epsilon_j)}} \tag{12}$$

with

$$F_{c,j}(R_{\mathrm{w}}) = F_c \frac{a^2}{A} = a^2 \sum_j^n f_j \left[\frac{\kappa}{2} (2/R_{\mathrm{w}} + c_{0,j})^2 + \bar{\kappa}/R_{\mathrm{w}}^2 \right] \tag{13}$$

the curvature free energy (5) per single component of lateral size a^2. ϵ_j is the component-particle interaction energy and $\tilde{\mu}_j$ is the chemical potential of component type j in the flat membrane area $\tilde{A}$. The chemical potential consists of the ideal contribution (logarithm of the density) and the excess part which contains the curvature free energy of a component embedded in a flat membrane. In general there are other contribution to the excess chemical potential, such as component interactions and membrane surface tension contribution. However, we assume that all other contributions remain constant upon particle wrapping, or at leat are negligible compared to the curvature contribution, and we only consider the curvature free energy changes.

The chemical potential is

$$\tilde{\mu}_j = k_{\mathrm{B}} T \ln(\tilde{f}_j) + f_{c,j}^0 \;, \tag{14}$$

with $f_{c,j}^0 \equiv f_{c,j}(\infty)$ the curvature free energy in a flat membrane ($R_{\mathrm{w}} \to \infty$). The adsorbed composition can, therefore, be written as

$$f_j^{\mathrm{w}} = \frac{\tilde{f}_j \, e^{\beta(f_{c,j}^0 - f_{c,j}(R_{\mathrm{w}}) - \epsilon_j)}}{\sum_j \tilde{f}_j \, e^{\beta(f_{c,j}^0 - f_{c,j}(R_{\mathrm{w}}) - \epsilon_j)}} = \tilde{f}_j \tilde{K}_j \;. \tag{15}$$

where in the last step we have defined an equilibrium constant

$$\tilde{K}_j = \frac{e^{\beta(f_{c,j}^0 - f_{c,j}(R_{\mathrm{w}}) - \epsilon_j)}}{\sum_j \tilde{f}_j \, e^{\beta(f_{c,j}^0 - f_{c,j}(R_{\mathrm{w}}) - \epsilon_j)}} \tag{16}$$

specifying how strong individual component types adsorb to the particle. The equilibrium constant $\tilde{K}_j$ is not to be confused with the Gaussian curvature K. Another conservation relation emerges: $\sum_j \tilde{f}_j \tilde{K}_j = 1$. Using Eqs. (10, 11, 15) we can write the composition of the remaining membrane as:

$$\tilde{f}_j = \frac{f_j}{1 + \frac{A_{\mathrm{w}}}{A}(\tilde{K}_j - 1)} \;. \tag{17}$$

The total free energy change upon a particle endocytosis can be written in terms of individual contributions due to membrane curvature, binding to the particle, mixing entropy and surface tension Π:

$$\Delta F = \Delta F_c + \Delta \epsilon - T \Delta S + \Pi A_{\mathrm{w}} \;. \tag{18}$$

The change in the curvature free energy upon endocytosis is obtained by the free energy of the wrapped membrane shell and the remaining flat membrane, minus the initial state which is a flat membrane of area A

$$\Delta F_c = F_c^{\mathrm{w}} + \tilde{F}_c - F_c = A_{\mathrm{w}} \frac{\kappa}{2} \sum_j f_j^{\mathrm{w}} (2/R_{\mathrm{w}} + c_{0,j})^2 + \tilde{A} \frac{\kappa}{2} \sum_j \tilde{f}_j (c_{0,j})^2 - A \frac{\kappa}{2} \sum_j f_j (c_{0,j})^2 + 4\pi \tilde{\kappa} \;. \tag{19}$$

This expression was obtained using Eq. (5) with the mean curvature determined by the shell radius $C = -1/R_{\mathrm{w}}$ for an endocytosed shell, and $C = 0$ for a flat membrane. The contribution of the Gaussian curvature is $4\pi \tilde{\kappa}$ due to Gauss-Bonnet theorem.

The change in binding interaction energy between membrane components and the particle is trivial:

$$\Delta\epsilon = \frac{A_\mathrm{w}}{\Delta a} \sum_j f_j^\mathrm{w} \epsilon_j \tag{20}$$

because the component-particle interaction vector $\boldsymbol{\epsilon}$ is a constant and interaction is only present in the final fully wrapped endocytosed state.

Lastly, the membrane is assumed to be in a fluid state. The mixing entropy of components is given by the Gibbs expression for the entropy per component: $s = -k_\mathrm{B} \sum_j f_j \ln(f_j)$, where we remember f_j as the fraction of component j in the membrane and k_B is the Boltzmann constant. f_j can also be seen as the probability that a randomly chosen component is of type j. The difference in entropy of mixing of different component types upon endocytosis is

$$\Delta S = S^\mathrm{w} + \tilde{S} - S = -\frac{k_\mathrm{B}}{a^2} \left[A_\mathrm{w} \sum_j f_j^\mathrm{w} \ln f_j^\mathrm{w} + \tilde{A} \sum_j \tilde{f}_j \ln \tilde{f}_j - A \sum_j f_j \ln f_j \right] \tag{21}$$

using the Gibbs entropy per single component and entropy extensivity $S = \frac{A}{a^2} s$.

These relations Eqs. (18-21) result in a closed form expression for the endocytosis free energy as a function of the membrane composition $\mathbf{f}$, curvature vector $\mathbf{c}_0$, interaction vector $\boldsymbol{\epsilon}$ and the wrapped membrane shell radius R_w:

$$\Delta F(\mathbf{f}, \mathbf{c}_0, \boldsymbol{\epsilon}, R_\mathrm{w}) = A_\mathrm{w} \sum_j f_j K_j \left[\frac{\epsilon_j}{a^2} + \frac{2\kappa}{R_\mathrm{w}} \left(\frac{1}{R_\mathrm{w}} + c_{0,j} \right) + \frac{k_\mathrm{B}T}{a^2} \ln(K_j) \right] + A_\mathrm{w}\Pi + 4\pi\bar{\kappa} + A_\mathrm{w}\mathcal{O}(A_\mathrm{w}/A) . \tag{22}$$

The first term inside the square brackets captures the binding of components to the particle, the second terms curvature mismatch penalty, and the third term the effect of the membrane composition change between the flat membrane and the wrapped part with the equilibrium constant

$$K_j = \frac{e^{-\beta\left[\epsilon_j + \frac{2\kappa a^2}{R_\mathrm{w}}(1/R_\mathrm{w} + c_{0,j})\right]}}{\sum_j f_j \, e^{-\beta\left[\epsilon_j + \frac{2\kappa a^2}{R_\mathrm{w}}(1/R_\mathrm{w} + c_{0,j})\right]}} . \tag{23}$$

The pre-factor $A_\mathrm{w} = 4\pi R_\mathrm{w}^2$ is the wrapped membrane area and a^2 the individual component lateral size. Finally, the last term $\mathcal{O}(A_\mathrm{w}/A)$ captures all terms of order A_w/A and higher. For a large membrane $A_\mathrm{w} \ll A$ these terms can be neglected.

E. Detailed derivation of endocytosis free energy

Here we provide a step by step derivation procedure of the endocytosis free energy Eq. (22) from Eqs. (18-21).

Firstly, we focus on the curvature free energy change Eq. (19). Inserting Eqs. (15) and (17) and $\tilde{A} = A - A_\mathrm{w}$, rearranging and canceling out a few terms we find

$$\Delta F_c = 2A_\mathrm{w}\kappa \sum_j \frac{f_j \tilde{K}_j}{1 + \frac{A_\mathrm{w}}{A}(\tilde{K}_j - 1)} \left(1/R_\mathrm{w}^2 + c_{0,j}/R_\mathrm{w} \right) . \tag{24}$$

The interaction energy contribution Eq. (20) is slightly rewritten by inserting Eqs. (15) and (17):

$$\Delta\epsilon = \frac{A_\mathrm{w}}{a^2} \sum_j \epsilon_j \frac{f_j \tilde{K}_j}{1 + \frac{A_\mathrm{w}}{A}(\tilde{K}_j - 1)} \tag{25}$$

Finally, the entropy change Eq. (21) is also rewritten by inserting Eqs. (15) and (17) and $\tilde{A} = A - A_\mathrm{w}$:

$$\frac{\Delta S}{k_\mathrm{B}} = -\frac{A_\mathrm{w}}{a^2} \sum_j \frac{f_j}{1 + \frac{A_\mathrm{w}}{A}(\tilde{K}_j - 1)} \left[\tilde{K}_j \ln \tilde{K}_j + \left(1 - \frac{A}{A_\mathrm{w}} - \tilde{K}_j \right) \ln \left(1 + \frac{A_\mathrm{w}}{A}(\tilde{K}_j - 1) \right) \right] \tag{26}$$

We now take the limit of a large membrane: $A_\mathrm{w}/A \to 0$. This implies: $\tilde{c}_j \to c_j$ (from Eq. (17)) and $\tilde{K}_j \to K_j$ (from Eq. (16)) where the equilibrium constant K_j is defined as:

$$K_j = \frac{e^{\beta(f_{c,j}^0 - f_{c,j}(R_\mathrm{w}) - \epsilon_j)}}{\sum_j f_j\, e^{\beta(f_{c,j}^0 - f_{c,j}(R_\mathrm{w}) - \epsilon_j)}} = \frac{e^{-\beta\left[\epsilon_j + \frac{2\kappa a^2}{R_\mathrm{w}}(1/R_\mathrm{w} + c_{0,j})\right]}}{\sum_j f_j\, e^{-\beta\left[\epsilon_j + \frac{2\kappa a^2}{R_\mathrm{w}}(1/R_\mathrm{w} + c_{0,j})\right]}} \ . \tag{27}$$

In the second step in the above equation the Helfrich free energy per component (Eq. (13)) was inserted. Taking the limit $A_\mathrm{w}/A \to 0$ the curvature free energy (24) becomes:

$$\Delta F_c = 2 A_\mathrm{w} \kappa \sum_j f_j K_j \left(1/R_\mathrm{w}^2 + c_{0,j}/R_\mathrm{w}\right) + A_\mathrm{w} \mathcal{O}(A_\mathrm{w}/A) \ . \tag{28}$$

The interaction energy (25):

$$\Delta\epsilon = \frac{A_\mathrm{w}}{a^2} \sum_j \epsilon_j f_j K_j + A_\mathrm{w} \mathcal{O}(A_\mathrm{w}/A) \ . \tag{29}$$

and the entropy (26) can be simplified by expanding the logarithm to the first order and using equalities $\sum_j f_j = 1$ and $\sum_j f_j K_j = 1$:

$$\frac{\Delta S}{k_B} = -\frac{A_\mathrm{w}}{a^2} \sum_j f_j K_j \ln K_j + A_\mathrm{w} \mathcal{O}(A_\mathrm{w}/A) \ . \tag{30}$$

$\mathcal{O}(A_\mathrm{w}/A)$ captures all terms of order A_w/A and higher. Summing up the individual contributions (Eq. (18)) the final result (Eq. (22)) follows.
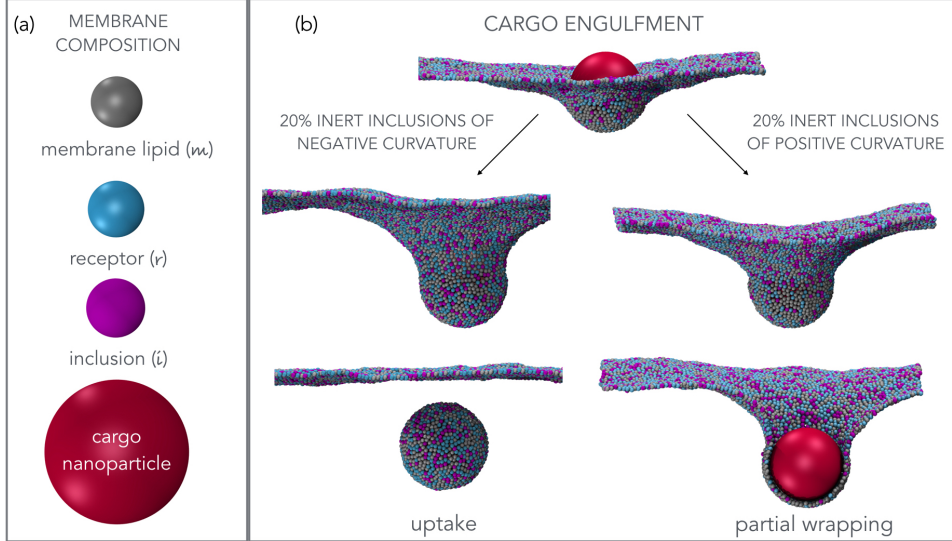
II.   SIMULATION MODEL

FIG. S1: **Simulation model**. (a) The membrane is composed of three types of beads: non-binding lipid beads ('m') of zero spontaneous curvature, cargo-binding receptor beads ('r') of spontaneous curvature $c_{0,\mathrm{r}}$, and inert (non-binding) inclusions ('i') of spontaneous curvature $c_{0,\mathrm{i}}$ [1]. The cargo (modelled as generic nanoparticle) is much bigger than either of the membrane beads. (b) Cargo binds to membrane receptors, deforms the membrane, and in case of 20% of inert inclusions of negative curvature becomes completely wrapped by the membrane and buds off, while in the case of 20% of inert inclusions of positive curvature it stays partially wrapped without being endocytosed within the time of the simulation of 10^7 time steps.

The membrane is modelled using a coarse grained one-particle thick model [1], which we implemented in the LAMMPS Molecular Dynamics package [2]. In short, in this model each membrane bead is described

by its position and an axial vector. The beads interact with a combination of an attractive potential that depends on the inter-bead distance and drives the membrane self-assembly, and an angular potential that depends on the angle between the axial vectors of neighbouring beads and mimics membrane bending rigidity. The spontaneous curvature per bead is implemented via a preferred angle between two axial vectors, θ_0, and is related to it via $c_0 \approx 2\sin(\theta_0/d_0)$. $d_0 \approx r_{\mathrm{cut}}^{\mathrm{bead-bead}}$ is the average distance between membrane beads, for membrane with very low tension the average distance will be located roughly at the minimum of the attractive potential. Following the notation from the original paper [1], we choose the parameters $\epsilon_{\mathrm{bead-bead}} = 4.34 k_{\mathrm{B}}T, \xi = 4, \mu = 3, r_{\mathrm{cut}}^{\mathrm{bead-bead}} = 1.12\sigma$ for all the membrane components, which positions our membrane in the fluid phase of the phase space. Using thermodynamic integration and theoretical considerations we determined the bending and Gaussian rigidity of this membrane model, $\kappa = -\bar{\kappa} = 22 k_{\mathrm{B}}T$, see Section III for details of the calculation. The mixing curvature terms between membrane beads i, j of different spontaneous curvatures are assumed to be symmetric $c_{0,ij} = \frac{c_{0,ii}+c_{0,jj}}{2}$, and hence, the spontaneous curvature does not lead to phase separation of components of different curvatures.

The cargo nanoparticle interacts with the membrane receptors via a shifted Lennard-Jones potential, where the cargo-receptor interaction strength is controlled by the binding affinity ϵ. The interaction between the cargo and any of the non-receptor beads is governed only by volume exclusion described by the Weeks-Chandler-Anderson potential:

$$U_{\mathrm{WCA}}(r) = \epsilon_{\mathrm{WCA}} \left[1 + 4 \left(\frac{\sigma}{r - R_{\mathrm{p}}} \right)^{12} - 4 \left(\frac{\sigma}{r - R_{\mathrm{p}}} \right)^{6} \right] , \tag{31}$$

for $0 \leq r - R_{\mathrm{p}} \leq 2^{1/6}\sigma$ and $U_{\mathrm{WCA}}(r) = 0$ otherwise. r is the bead to particle centre-of-mass distance, R_{p} and σ are the nanoparticle and bead radius, respectively. We chose the interaction strength $\epsilon_{\mathrm{WCA}} = \epsilon_{\mathrm{bead-bead}}$.

The interaction potential between nanoparticle and 'receptor' membrane beads is modelled as a cut-and-shifted Lennard Jones potential

$$U_{\mathrm{bead-particle}}(r) = 4\epsilon^* \left[\left(\frac{\sigma}{r - R_{\mathrm{p}}} \right)^{12} - \left(\frac{\sigma}{r - R_{\mathrm{p}}} \right)^{6} \right] + U_{cs} , \tag{32}$$

for $r - R_{\mathrm{p}} \leq 2.6\sigma$ and 0 otherwise. $U_{cs} = -U_{\mathrm{bead-particle}}(2.6\sigma)$.

We simulated a flat square portion of a membrane made of 49920 beads with periodic boundary conditions in a NpH ensemble with pressure $p = -10^{-4} k_{\mathrm{B}}T/\sigma^3$ to model a membrane with very low tension. The simulation box height was fixed at $L_z = 200$. The surface tension of the membrane is therefore $\Pi = -pL_z = 2 \cdot 10^{-2} k_{\mathrm{B}}T/\sigma^2$. The component size being $\sigma \approx 5$nm results in $\Pi \approx 10^{-3} k_{\mathrm{B}}T/\mathrm{nm}^2$, which is at a lower end of biological surface tensions [3]. All the particles in the system are in addition subject to random noise implemented via the Langevin thermostat with friction coefficient set to unity: $\gamma = m/\tau$, where m is the bead mass (set to unity) and τ the simulation unit of time. To capture the correct dynamics the cargo nanoparticle parameters are rescaled accordingly: mass of nanoparticle is $m_{\mathrm{p}} = 8(R_{\mathrm{p}}/\sigma)^3$ and nanoparticle friction coefficient $\gamma_{\mathrm{p}} = 2R_{\mathrm{p}}/\sigma$.

The initial condition of all simulations is a flat membrane with beads arranged on a hexagonal lattice with a randomly chosen permutation of bead identities (types) and the location of the cargo particle's centre of mass $R_{\mathrm{p}} + 2\sigma$ above the membrane. All quantities are expressed in terms of the membrane bead diameter σ, which corresponds to $\sigma = 5$nm in physical units. The bead density for a flat membrane was measured to be $\rho_{\mathrm{beads}} = 1.21\sigma^{-2}$, which provides a mapping with a theoretical component size $a = \sigma/\sqrt{1.21}$.

The endocytosis is monitored through the wrapping coverage of the cargo by the membrane beads, where the wrapping is defined as:

$$w_j = \frac{N_j^{\mathrm{contact}}\sqrt{3}}{8\pi(R_{\mathrm{p}}/\sigma + 1)^2}, \tag{33}$$

with N_j^{contact} being the number of membrane beads of type j whose centre-of-mass distance to the particle centre is less than $R_{\mathrm{p}} + \sigma$. The total wrapping is $w = \sum_j w_j$. Since we sometimes observe uptake of non-completely wrapped nanoparticles ($w < 1$), we chose to consider a nanoparticle endocytosed if $w > 0.8$ and its centre-of-mass is located below the fully healed mother membrane. The length of each simulation was 10^7 steps with a time step of 0.008τ, where τ is the unit of time.

A. determining phase boundaries

For the simulation data points the phase boundaries were determined by simulating the cargo-membrane system for a range of cargo-receptor interaction energies ϵ (Figure 3(a)) and finding the minimal interaction energy ϵ^* where the cargo becomes endocytosed ($w > 0.8$ and particle centre-of-mass below the fully healed mother membrane). The procedure was then repeated for different receptor curvatures. Analogously, the same procedure was done in Figure 3(b) where we were looking for a minimal fraction of receptors where the endocytosis occurs, at various fraction of inert inclusions and inclusion curvatures. The search step sizes were $\delta\epsilon = 0.1k_{\mathrm{B}}T$ and $\delta f_{\mathrm{r}} = 0.01$.

For the analytical phase boundaries shown on Figures 3 and 4 we numerically self-consistently solve the Eq. (22) by keeping $\Delta F = 0$. We employ FindRoot function in Wolfram Mathematica to find the value of the interaction energy ϵ (Figure 3A) or the receptor fraction f_{r} (Figure 3B) for which the expression in Eq. (22) equals to zero.

III. DETERMINING GAUSSIAN BENDING STIFFNESS

The standard bending rigidity κ can be obtained from the fluctuation spectrum of the membrane. the Gaussian bending rigidity $\bar{\kappa}$, however, is trickier to calculate. We obtain the Gaussian bending rigidity of the membrane model both by theoretical considerations and by performing thermodynamic integration. Both approaches are presented below, theoretical considerations yield $\bar{\kappa} = -\kappa$ and thermodynamic integration $\bar{\kappa} \approx -\kappa \approx -22k_{\mathrm{B}}T$ which also agrees with the value obtained from the membrane fluctuation spectrum [1]. We, therefore, use $\bar{\kappa} = -\kappa = 22k_{\mathrm{B}}T$ when comparing analytical and simulation results.

A. Thermodynamic integration

We performed Monte Carlo simulations with thermodynamic integration scheme to calculate the mean κ and Gaussian $\bar{\kappa}$ bending rigidity of the membrane. Three sets of simulations with different membrane topologies were performed: flat membrane (periodic boundary in lateral directions), cylindrical membrane (periodic boundary in the cylinder axis) and spherical membrane. $N = 5000$ beads were used for all simulations and no applied external pressure, $5 \cdot 10^5$ MC cycles were used for all simulations, unless noted otherwise. The radius of the cylindrical membrane was half the radius of a spherical membrane $R_{\mathrm{c}} = R_{\mathrm{s}}/2$. Such a choice allows us to directly determine the bending rigidities from the free energies of the three different membrane configurations

$$\kappa = \frac{F_{\mathrm{c}} - F_{\mathrm{f}}}{8\pi} , \qquad \bar{\kappa} = \frac{F_{\mathrm{s}} - F_{\mathrm{c}}}{4\pi} , \tag{34}$$

where F_{f}, F_{c} and F_{s} are the free energies of the membrane in the flat, cylindrical and spherical configuration, respectively.

The flat membrane 2D density was measured to be $\rho_{\mathrm{beads}} = 1.206$ at vanishing tension (no applied lateral pressure). Therefore we chose the spherical membrane radius as $R_{\mathrm{s}} = \sqrt{\frac{N}{4\pi\rho}}$ and the cylindrical membrane radius $R_{\mathrm{c}} = R_{\mathrm{s}}/2$, with the cylinder height chosen to conserve the number of beads $h_{z,\mathrm{c}} = \frac{N}{2\pi R_{\mathrm{c}}\rho_{\mathrm{beads}}}$.

The reference state of the thermodynamic integration is a 2D ideal gas with density $\rho_{\mathrm{beads}} = 1.206$ confined to lie on a flat, cylindrical or spherical surface. The free energy of the thermodynamic integration proceeded in two steps. First the bead-bead interaction potential strength was increased from 0 (ideal gas) to $\epsilon_{\mathrm{bead-bead}} = 4.34k_{\mathrm{B}}T$. A total of 201 simulations were performed for each topology with the interaction parameter linearly spaced $\epsilon_{i,\mathrm{bead-bead}} = \epsilon_{\mathrm{bead-bead}}\frac{i}{200}$. The first calculation ($i = 0$) was performed at $\epsilon_{0,\mathrm{bead-bead}} = 0.001k_{\mathrm{B}}T$. The results of these simulations are shown on Figure S2a). The integration was performed on the energy differences between different membrane topologies which avoids the problem of integrand divergence at $\epsilon \sim 0$. The thermodynamic integration using Simpson's rule yields bending rigidities $\kappa_{\mathrm{2D}} = 23.2k_{\mathrm{B}}T$ and $\bar{\kappa}_{\mathrm{2D}} = -25.5k_{\mathrm{B}}T$. Note that the membrane beads were confined to a 2D surface.

In the second thermodynamic integration step the membrane beads are relaxed to allow for fluctuations in the direction normal to the membrane. A harmonic confining potential $U(r) = \frac{k}{2}r^2$ is introduced for each bead, with r the normal distance between the bead and the confining surface. The confining
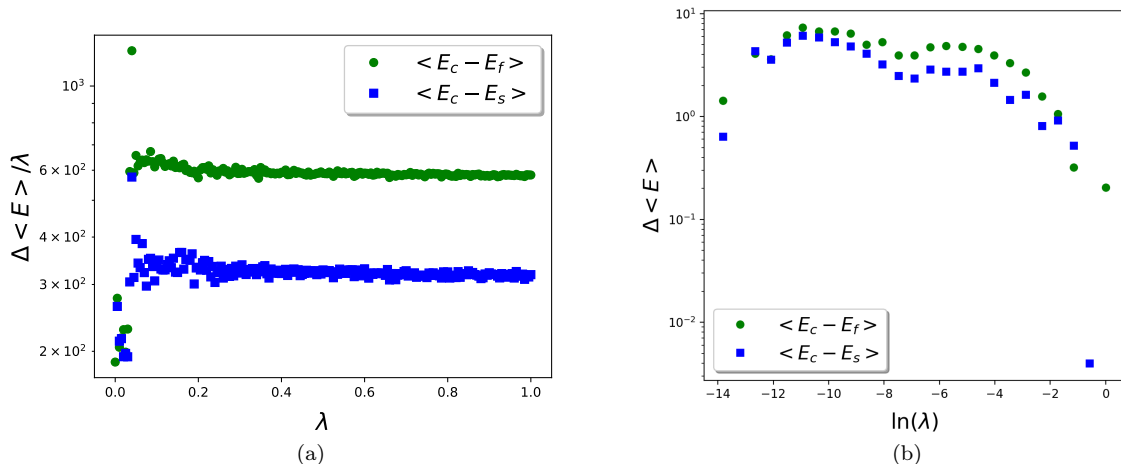
FIG. S2: Thermodynamic integration results. Average potential energy difference between different membrane topologies as a function of the thermodynamic integration parameter λ. E_f, E_c and E_s denote the potential energies of the three distinct topologies (flat, cylindrical, spherical). (a) The first thermodynamic integration step: changing the bead-bead interaction $\lambda = \epsilon_{i,\text{bead}-\text{bead}}/\epsilon_{\text{bead}-\text{bead}}$, and (b) The second thermodynamic integration step: changing the harmonic confining potential $\lambda = k_i/k_{\max}$.

surfaces are identical to the surfaces used above (flat, cylinder, sphere). 25 values for the confining potential strength k are logarithmically spaced between $k_{\min} = 0.01 k_\text{B}T/\sigma^2$ and $k_{\max} = 10000 k_\text{B}T/\sigma^2$. Thermodynamic integration yields the correction to the bending rigidities: $\kappa_{\text{relax}} = -2.0 k_\text{B}T$ and $\bar{\kappa}_{\text{relax}} = 3.0 k_\text{B}T$.

The bending rigidities of the membrane are therefore:

$$\kappa = \kappa_{2D} + \kappa_{\text{relax}} = 21.2 k_\text{B}T \ , \tag{35}$$

$$\bar{\kappa} = \bar{\kappa}_{2D} + \bar{\kappa}_{\text{relax}} = -22.5 k_\text{B}T \ . \tag{36}$$

The value for κ obtained by thermodynamic integration agrees well with the bending rigidity calculated from the fluctuation spectrum $\kappa_{\text{fs}} \approx 22 k_\text{B}T$ [1].

B. Analytical considerations

The Gaussian bending rigidity can also be estimated assuming a simple microscopic model of the membrane. The membrane consists of a monolayer of beads. Individual beads are not deformable and have cylindrically symmetry around a director axis. Nearest neighbour beads i, j have a harmonic pair potential with spring constant k for the director bending

$$U_{ij} = \frac{k}{2}(\theta_{ij} - \theta_0)^2 \ , \tag{37}$$

where θ_{ij} is the angle between the directors of the two beads and θ_0 is a constant specifying the preferred orientation between the two beads. Mean distance between nearest neighbours is d_o and each bead has z nearest neighbours. The angle between neighbouring beads is related to the membrane curvature: $\sin(\theta_{ij}/2) = d_0/(2R_{ij})$ from which we obtain for small curvatures $\theta_{ij} \approx d_0/R_{ij} = d_0 C_{ij}$, with $R_{ij} = 1/C_{ij}$ the radius of the curved membrane with curvature C_{ij}. Therefore, the above equation can be rewritten to

$$U_{ij} = \frac{kd_0^2}{2}(C_{ij} - c_0)^2 \ , \tag{38}$$

with the spontaneous curvature $c_0 = \theta_0/d_0$.

Using this microscopic model we can calculate the macroscopic bending rigidities κ and $\bar{\kappa}$ by comparing the energy of bending obtained from the microscopic model with the Helfrich hamiltonian. For a flat membrane $C_{ij} = 0$ the microscopic model yields the membrane elastic energy per bead

$$U^{\text{flat}} = \frac{z}{2} \frac{kd_0^2}{2} (c_0)^2 . \tag{39}$$

The prefactor $\frac{z}{2}$ is simply the number of pair interactions per bead. Cylindrical membrane yields the elastic energy of

$$U_{\text{bend}}^{\text{cylinder}} = \frac{z}{4} \frac{kd_0^2}{2} (c_0)^2 + \frac{z}{4} \frac{kd_0^2}{2} (1/R_{\text{c}} - c_0)^2 \tag{40}$$

using a mean-field like approximation where half of the nearest neighbours are parallel $C_{ij} = C_1 = 0$ and the other half are confined to a curvature of $C_{ij} = C_2 = 1/R_{\text{c}}$ with R_{c} the cylinder radius and C_1, C_2 the principal curvatures of the membrane. Lastly, spherical membrane results in

$$U_{\text{bend}}^{\text{sphere}} = \frac{z}{2} \frac{kd_0^2}{2} (1/R_{\text{s}} - c_0)^2 \tag{41}$$

because all nearest neighbours feel the same bending curvature $C_{ij} = C_1 = C_2 = 1/R_{\text{s}}$ and R_{s} is the sphere radius.

The Helfrich expression for the elastic free energy density is

$$H = \frac{\kappa}{2} (2C - c_0)^2 + \bar{\kappa} K \tag{42}$$

where $C = (C_1 + C_2)/2$ is the mean curvature of the membrane and $K = C_1 C_2$ the Gaussian curvature with C_1 and C_2 the principal curvatures of the membrane. For a flat membrane Helfrich yields $H^{\text{flat}} = \frac{\kappa}{2}(c_0)^2$, cylindrical $H^{\text{cylinder}} = \frac{\kappa}{2}(1/R_{\text{c}} - c_0)^2$ and spherical $H^{\text{sphere}} = \frac{\kappa}{2}(2/R_{\text{s}} - c_0)^2 + \bar{\kappa}/R_{\text{s}}^2$.

The elastic energy obtained from the microscopic model must be the same as the Helfrich expression for all three membrane topologies up to a common additive constant. Assuming that the membrane curvature radii considered are always large as compared to the microscopic bead size, $d_0/R \sim 0$, the local configuration of beads will not be affected by the curvature and the number of neighbours per bead z can be treated as a constant. Hence, the only possible relation connecting Eqs. (39-42) is

$$\kappa = -\bar{\kappa} = \frac{zkd_0^2}{4} \tag{43}$$

and $U = H + \frac{\kappa}{2} c_0^2$.

Therefore, for a membrane composed of a monolayer of cylindrically symmetric beads and small curvatures the Gaussian bending rigidity is opposite of the mean bending rigidity $\bar{\kappa} = -\kappa$. This result is supported by the thermodynamic integration discussed above. We therefore use the value of bending rigidities of $\bar{\kappa} = -\kappa = 22 k_{\text{B}} T$ for both the mean and Gaussian bending rigidity when comparing analytical and simulation results of nanoparticle endocytosis.

IV. SUPPORTING RESULTS

A. Membrane stability

Analytical model can provide insight into membrane stability depending on the composition of curved inclusions. We consider only the membrane, without cargo, and determine the thermodynamic stability of a flat membrane with respect to budding and formation of a separate vesicle. Eq. (22) is solved numerically to obtain inert inclusion curvature as a function of the vesicle radius R_{w}: $c_{0,\text{i}}(R_{\text{w}}|\Delta F = 0)$ in the limiting case of zero free energy cost of forming the vesicle. Phase diagrams on Figure S3 show that a flat membrane with zero total spontaneous curvature is thermodynamically stable if the absolute value of spontaneous curvature of individual components is not large. The larger the fraction of curved components f_{i} the lower the limiting value of spontaneous curvature $c_{0,\text{i}}$. On the other hand, flat membranes with non-zero total spontaneous curvature are, as expected, always unstable with respect to a formation of a vesicle.
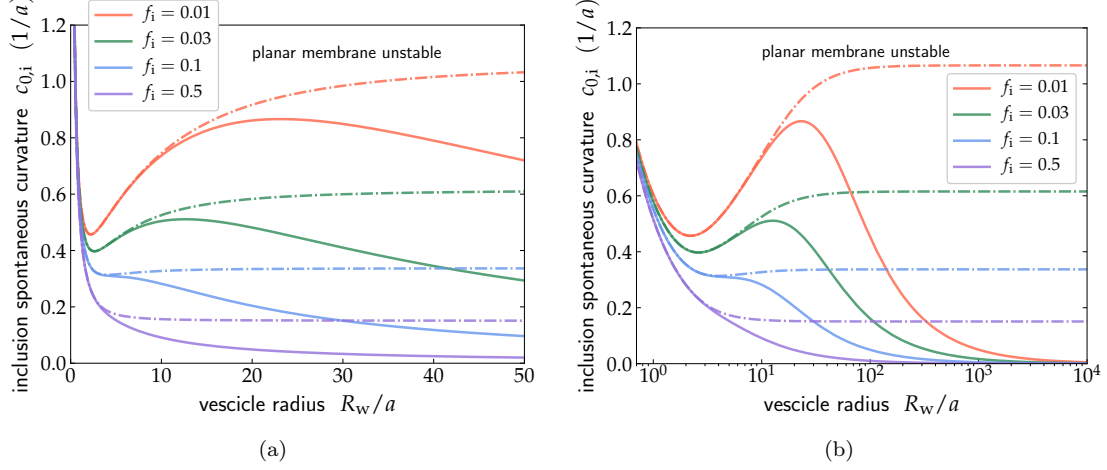
(a)

(b)

FIG. S3: phase diagram of membrane stability. a) shows the linear and b) the logarithmic plot of the same data. Solid lines correspond to a membrane with a fraction f_i of inclusions with absolute spontaneous curvature $c_{0,i}$. Any point above the solid line thermodynamically unstable with respect to the vesicle formation and the flat membrane is only metastable. In the limit of large vesicles ($R_w \to \infty$) the lines converge to zero ($c_{0,i} \to 0$) meaning that a flat membrane is always thermodynamically unstable. Dot-dashed lines show the corresponding phase plots where two types of inclusions are present such that the total spontaneous curvature of the membrane is zero: $c_{0,i'} = -c_{0,i}$ and $f_{i'} = f_i$. In this case the phase plots converge to a finite value of spontaneous curvature for large vesicles indicating that a flat membrane is thermodynamically stable. Parameters: $f_r = 0.0$, $\kappa = -\bar{\kappa} = 22 k_B T$.
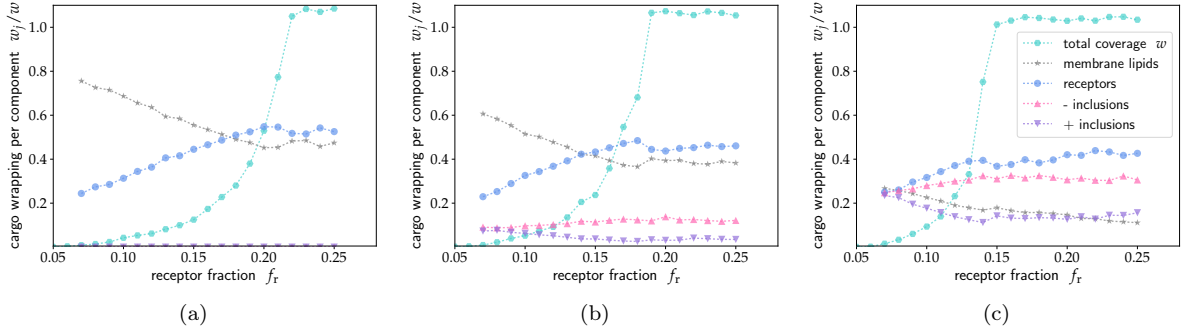

(a)

(b)

(c)

FIG. S4: Recruiting of different types membrane inclusions. The turquoise hexagons on all three plots correspond to data on Figure 5A in the main text for a) $f_i = f_{i'} = 0$, b) $f_i = f_{i'} = 0.1$ and c) $f_i = f_{i'} = 0.3$. The grey stars, blue circles, pink and purple triangles show the fraction of beads of specific type in contact with the nanoparticle. Clearly, the receptor beads and negatively curved inclusions are recruited to the particle, while membrane beads and positively curved inclusions are expelled. Receptor fraction $f_r = 0.2$ and membrane bead fraction is $f_m = 1 - f_r - 2f_i$.

B. Kinetics of endocytosis

On Figure S4 we show additional simulation results complementing Figure 4 in the main text. Furthermore, Figure. S5 shows the scaling of endocytosis rate with the particle size. The system size effects on Figure S6 demonstrate that the endocytosis rate also depends on the total membrane size. The shift, however, seems to be roughly constant for particle larger than $R_p > 10\sigma$. **Lateral pressure is kept constant in all simulations, the membrane surface tension, however, can also depends on the total simulated membrane size, (TC) cite system size effects in membrane surface tension, not sure about this, ask Daan**, to which we attribute the shift in endocytosis rate with system size. The increases selectivity effect discussed on Figure 5 of the main text remains regardless of the membrane size, as long as $L \gg R_p$. Note that the bead size in real units is about $\sigma \approx 5$nm, therefore, at the largest simulated membrane the size would be $\approx 3\mu$m; a length-scale comparable to the total cell membrane.
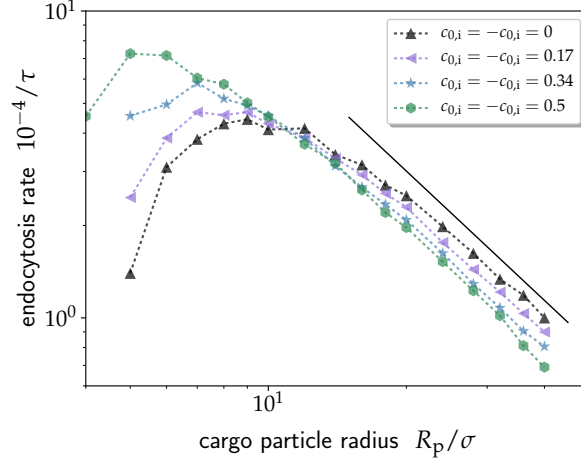
FIG. S5: **Endocytosis rate depends non-monotonically on the particle size.** a) Logarithmic plot of the data on Figure 5 in the main text. The black solid line indicates the power law scaling $k_r \propto R_p^{-\gamma}$ with the scaling exponent $\gamma = 1.4$.
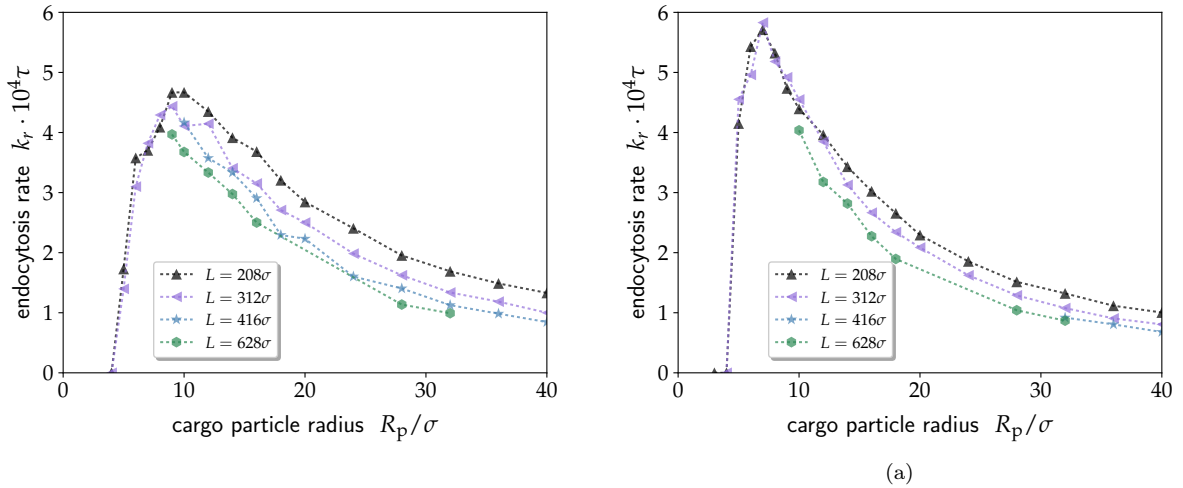

(a)

FIG. S6: **Membrane size effect** The endocytosis rate for different initial system sizes L. The number of membrane beads in the simulation is $N = \frac{15}{13}L^2$, the fraction 1513 was chosen because it well approximates the factor $\approx 2/\sqrt{3}$ which arises when positioning beads on a triangular lattice. a) $f_i = 0$, b) $f_i = f_{i'} = 0.2$. Other parameters, $c_r = 0.4$, $c_i = 0.2$, The data at $L = 312\sigma$ corresponds to the main plot of Figure 5 in the main text.

To further rationalise the enhanced sensitivity to cargo size when inclusions of both curvatures are present in the same amount, let us analyse the energetics of the neck of the membrane bud. The neck will be composed of two principal curvatures - the curvature parallel to the cargo-membrane contact line, and the curvature perpendicular to it. Following [4], we define the effective adhesive length, R_{adh}, which for the parameters used in Figure 5 of the main text is approximately $R_{adh} = \sqrt{2\kappa/|W|} \approx 5\sigma$, with $\kappa = 22k_BT$ and the effective adhesion $|W| = \frac{\epsilon}{\sigma^2} \frac{f_r e^{-\beta\epsilon}}{1+f_r e^{-\beta\epsilon}} \approx 2k_BT/\sigma^2$. The adhesive length R_{adh} determines the principal curvature perpendicular to the contact line in the neck $C_1 = 1/R_{adh}$, while the principal curvature parallel to the contact line is determined by the particle size $C_2 = -1/R_p$. For large cargoes, when $R_p \gg R_{adh}$, the mean curvature in the neck is positive, which makes it populated by positive inclusions, hampering endocytosis. For cargoes that satisfy $R_p \approx R_{adh}$, the mean curvature in the neck vanishes, and the negatively curved inclusions can freely diffuse into the membrane area wrapped around the cargo, enhancing endocytosis. This analysis is supported by monitoring the neck region composition shown on Figure S7. For large particles ($R_p = 32\sigma$) the neck composition is strongly dominated by positive inclusions, while for small particles ($R_p = 5\sigma$) the neck region has approximately equal fraction of both positive and negative inclusions. Interestingly, the composition of the wrapped

shell shows opposite tendency: For large particles the fraction of inclusion types adsorb is approximately the same, while for small particles the adsorption of positive inclusions is suppressed.
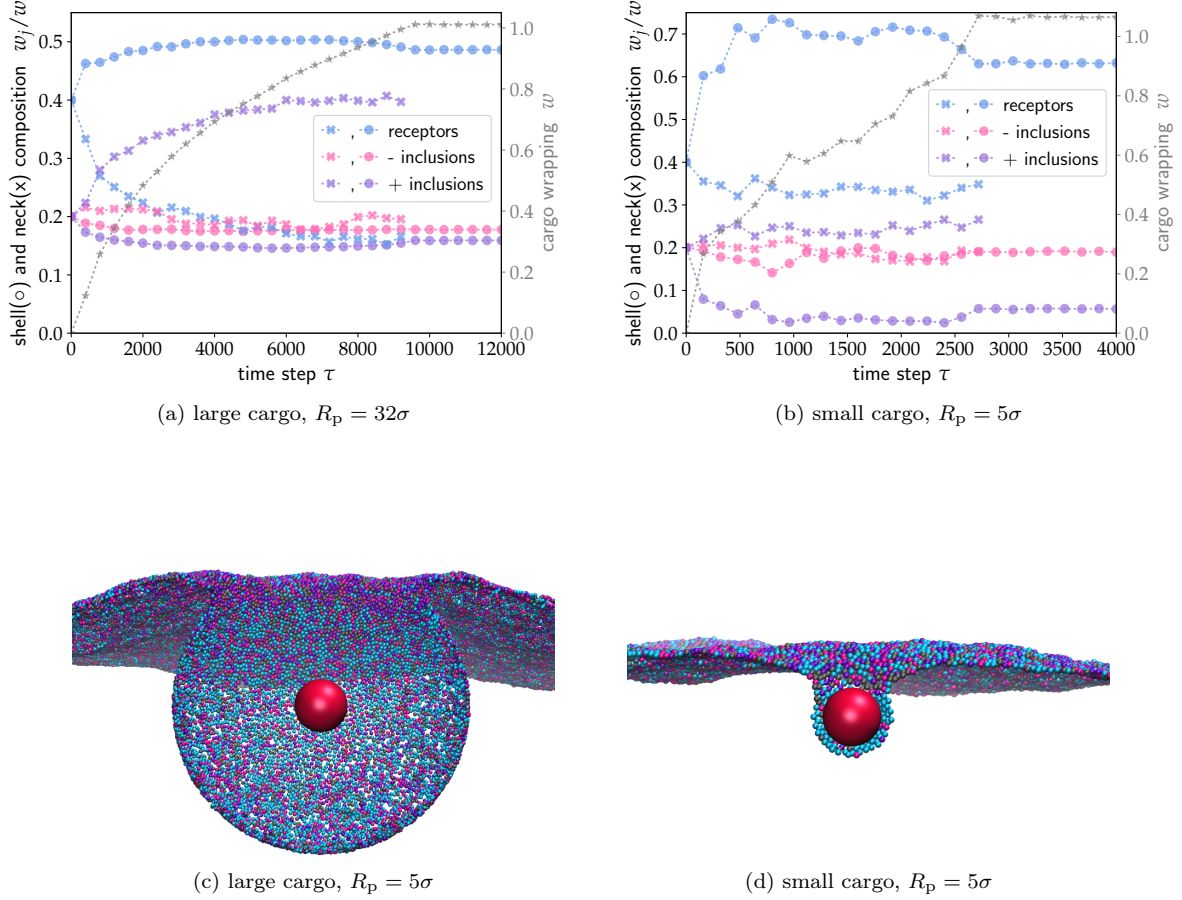

(a) large cargo, $R_\mathrm{p} = 32\sigma$

(b) small cargo, $R_\mathrm{p} = 5\sigma$

(c) large cargo, $R_\mathrm{p} = 5\sigma$

(d) small cargo, $R_\mathrm{p} = 5\sigma$

FIG. S7: **Analysis of the composition of the membrane neck as the endocytosis proceeds**. In a) and b) the circles denote the composition of the membrane shell wrapped around the cargo while the crosses show the composition of the membrane neck. Receptor beads are coloured blue, negative inclusions are pink color and positive inclusions purple. The cut-through snapshots parallel to the membrane plane on c) and d) correspond to plots on a and b), respectively, at cargo wrapping of approximately $w = 0.75$. The color scheme matches the symbol colors in a) and b), membrane (lipid) beads are colored grey. Note that the cargo size in c) has depicted using a significantly smaller radius for better visualisation of the wrapped membrane shell. The wrapped shell is defined as all beads within distance 1.5σ of the particle surface. The neck region is defined as all particles between a distance $1.5\sigma - 8\sigma$ of the particle surface. Grey stars show the total cargo wrapping (right axis) indicating the progression of endocytosis. Parameters correspond to Figure 5 in the main text: $f_\mathrm{r} = 0.4$, interaction $\epsilon_\mathrm{r}^* = 2.5 k_\mathrm{B}T$ and curvature $c_{0,\mathrm{r}} = 0$. The inclusion fraction is $f_\mathrm{i} = f_\mathrm{i'} = 0.2$ with opposite spontaneous curvatures $c_{0,\mathrm{i}} = -c_{0,\mathrm{i'}} = 0.34/\sigma$.

References

[1] Yuan, H.; Huang, C.; Li, J.; Lykotrafitis, G.; Zhang, S. *Phys. Rev. E* **2010**, *82*, 011905–1–011905–8.

[2] Plimpton, S. *J. Comput. Phys.* **1995**, *117*, 1–19.

[3] Zhang, S.; Li, J.; Lykotrafitis, G.; Bao, G.; Suresh, S. *Adv. Mater.* **2009**, *21*, 419–424.

[4] Agudo-Canalejo, J.; Lipowsky, R. *ACS Nano* **2015**, *9*, 3704–3720.